The Impact of Load Models in an Algorithm for Improving Voltage Stability via Demand Response

Mengqi Yao, Daniel K. Molzahn, and Johanna L. Mathieu

***Abstract*— Increasing communication and control capabilities will allow future power system operators to exploit large quantities of responsive demand. This paper discusses ongoing work that employs demand response to improve voltage stability via virtual spatial shifting of loads (i.e., altering the locational distribution of power consumption in one time period with an energy payback in a following time period). In this paper, we study the impact of load models on a previously proposed iterative linearization algorithm to determine loading patterns that maximize a voltage stability margin, namely, the smallest singular value (SSV) of the power flow Jacobian matrix. Specifically, we extend the algorithm to enable inclusion of composite load models consisting of both "ZIP" components and a steady-state squirrel-cage induction machine (IM) model. We then investigate the impact of different load models on both the stability margin and the loading pattern. Using the IEEE 14-bus system as an illustrative example, the results show that the type of load model affects the nominal system's SSV, the optimal SSV, and the optimal loading pattern. The maximum-achievable percent change in SSV is larger using IM models than using ZIP models. We also discuss the difficulty in interpreting the stability margin when the system undergoes structural changes resulting from the use of different voltage-dependent load models.**

NOTATION

Sets

$\mathcal{N}$	Set of all buses
$\mathcal{S}_{\mathrm{PV}}$	Set of all PV buses
$\mathcal{S}_{\mathrm{PQ}}$	Set of all PQ buses
$\mathcal{S}_{\mathrm{DR}}$	Set of buses with demand-responsive loads

Functions

$\mathcal{F}_k^P(\cdot)$	Real power injection at bus k
$\mathcal{F}_k^Q(\cdot)$	Reactive power injection at bus k
$\mathcal{F}_k^{ZP}(\cdot)$	Real power demand of ZIP load at bus k
$\mathcal{F}_k^{ZQ}(\cdot)$	Reactive power demand of ZIP load at bus k
$\mathcal{F}_k^{IP}(\cdot)$	Real power demand of IM at bus k
$\mathcal{F}_k^{IQ}(\cdot)$	Reactive power demand of IM at bus k
$\mathcal{H}_{kl}(\cdot)$	Line flow for line (k,l)

Variables & Parameters

J	Jacobian matrix
θ_k	Voltage angle at bus k
V_k	Voltage magnitude at bus k
$\theta_{\mu,k}$	Stator voltage angle of IM at bus k
$V_{\mu,k}$	Stator voltage magnitude of IM at bus k
$\theta_{\rho,k}$	Rotor voltage angle of IM at bus k
$V_{\rho,k}$	Rotor voltage magnitude of IM at bus k
s_k	Slip of IM at bus k
$R_{s,k}$	IM stator's resistance at bus k
$X_{ls,k}$	IM stator's leakage reactance at bus k
$R_{r,k}$	IM rotor's resistance at bus k
$X_{lr,k}$	IM rotor's leakage reactance at bus k
$X_{m,k}$	IM mutual reactance at bus k
Y	System admittance matrix
$P_{g,k}$	Real power generation at bus k
$P_{d,k}$	Real power demand at bus k
$Q_{g,k}$	Reactive power generation at bus k
$Q_{d,k}$	Reactive power demand at bus k
$S_{d,k}$	Total complex power demand at bus k
$S_{\mathrm{ZIP},k}$	Complex power demand of ZIP load at bus k
$S_{\mathrm{IM},k}$	Complex power demand of IM at bus k
κ_{kl}	Apparent power line limit for line (k,l)
λ	Eigenvalue of a matrix
u	Normalized right eigenvector
w	Normalized left eigenvector
ε_k	Ratio used for the ZIP model
n	Size of $\mathcal{N}$
n_{pv}	Size of $\mathcal{S}_{\mathrm{PV}}$
n_{pq}	Size of $\mathcal{S}_{\mathrm{PQ}}$
n_{dr}	Size of $\mathcal{S}_{\mathrm{DR}}$
a_1, a_2, a_3	ZIP load model real power coefficients
b_1, b_2, b_3	ZIP load model reactive power coefficients

Bold symbols denote vectors including all variables of a type. Overlines and underlines represent the upper and lower limits for a variable. Subscript "ref" denotes the slack bus. Superscript "0" denotes the nominal value. Superscript "T" denotes the transpose of a matrix. Superscript "*" denotes the conjugate of a matrix. The notation $X \succeq 0$ indicates that X is a positive semidefinite matrix.

I. INTRODUCTION

Improving communication and control capabilities within electric power systems makes the coordination of demand-responsive loads increasingly practical [1]. Significant research efforts have focused on using demand response to improve power system frequency stability by temporally shifting load, e.g., [2], [3]. Demand response could also be employed to improve static voltage stability, which describes the distance to voltage collapse. For example, [4] and [5] use load shedding to improve voltage stability, where the latter uses the loading margin as the static voltage stability margin. The smallest singular value (SSV) of the power flow Jacobian matrix has also been used as a stability

This work was supported by NSF Grant EECS-1549670 and the U.S. DOE, Office of Electricity Delivery and Energy Reliability under contract DE-AC02-06CH11357. M. Yao and J.L. Mathieu are with the Department of Electrical Engineering and Computer Science at the University of Michigan, {myao,jlmath}@umich.edu. D.K. Molzahn is with Argonne National Laboratory, dmolzahn@anl.gov.

margin in, e.g., [6]–[8]. The SSV measures the distance from the current operating point to the boundary of the feasible operating region, as described by the power flow equations. References [9] and [10] formulate Optimal Power Flow (OPF) problems that incorporate voltage stability constraints based on the SSV, ensuring that the resulting operating point is an adequate distance from the feasibility boundary.

Our recent work [11] develops an algorithm to maximize the SSV of the power flow Jacobian via virtual spatial load shifting, which is achieved by altering the locational distribution of power consumption for a short period of time. The total load is kept constant (with the exception of small changes in system losses) so that frequency stability is unaffected. This is followed by a period during which the increases/decreases in consumption of specific loads are paid back so that the each load receives adequate energy over the full interval. Using an iterative linearization technique, the approach in [11] solves an optimization problem that determines a loading pattern that maximizes the SSV of the power flow Jacobian matrix. The loads are modeled as constant power demands (i.e., the demands are independent of the voltage magnitudes), with a fixed power factor.

Proper load models are particularly important in stability studies [12]–[15]. This paper extends the algorithm from [11] to enable inclusion of voltage-dependent load models, specifically ZIP models (i.e., real and reactive demand models with constant impedance, constant current, and constant power components) and steady-state squirrel-cage induction machine (IM) models. Inclusion of these models changes the power flow Jacobian, altering the nominal SSV. We investigate the impact of these models on the optimal SSV and optimal loading pattern. Of course, in practice, we do not choose the load model, but rather identify it using system data, e.g., from Phasor Measurement Units [16]–[18]. Given this, our results are useful for two reasons: 1) they help us understand which types of systems (as defined by the load mix) might benefit more or less from using demand response to improve the SSV, and 2) they help us determine the difference in loading pattern and optimality loss we would obtain if we were to use simple load models (e.g., constant power load models) instead of detailed load models within our algorithm.

The contributions of this paper are as follows: 1) we extend the SSV maximization problem in [11] to include voltage-dependent load models, 2) we extend the iterative linear programming approach used in [11] to solve this problem, 3) we compare the solutions and optimal SSVs associated with different types of load models, and 4) we discuss difficulties in interpreting the stability margin when the system undergoes structural changes resulting from the use of different load models.

This paper is organized as follows. Section II conceptually describes our approach for improving the voltage stability margin. Section III details the ZIP and induction machine models. Section IV presents the SSV maximization problem and our solution algorithm. Section V shows several case studies and their results. Section VI concludes the paper.

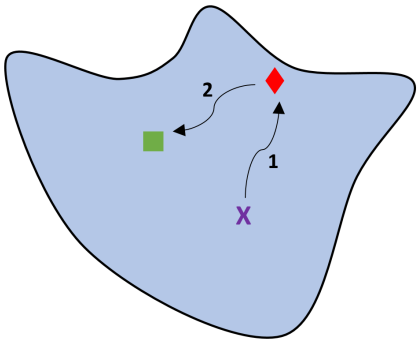

Fig. 1. Conceptual description of the problem. The blue area represents the stability region. The purple X shows the initial operating point, the red diamond shows the operating point after a disturbance, and the green square shows the operating point after an optimal change in loading pattern.

II. Problem Description

Fig. 1 conceptually describes our approach for improving the voltage stability margin. The blue shaded region represents the feasible operating region. The system is initially operating at a stable point (at the purple X). A disturbance causes the system to move along Path 1, resulting in operation near the feasibility boundary (at the red diamond). Our algorithm computes a change to the locational distribution of the demand-responsive load. Specifically, we increase some loads and decrease others while ensuring that the total real power consumption of the loads and real power production of each generator (with the exception of the slack bus, which compensates for the change in system losses) is constant so as not to affect the system's frequency stability. The reactive power consumption of the demand-responsive loads changes based on the load model. The reactive power production of the generators adjusts to the new loading pattern in order to keep the voltage magnitudes at generator buses constant. This moves the operating point away from the boundary along Path 2 (to the green square).

After a short period of time, the system is redispatched to "pay back" the energy deficit/surplus of each demand-responsive load. Specifically, loads that increased consumption now decrease consumption, and vice versa, such that the total energy consumed by each load over the full interval is equivalent to its baseline consumption. The redispatch should not only compensate for the demand response actions but also maintain or improve the voltage stability margin. After the energy payback period, the operating point either returns to the initial operating point (purple X) or moves to another point with an adequate stability margin.

Like [11], this paper focuses on computing loading patterns that improve the voltage stability margin and leaves the redispatch step to future work. In contrast to [11], this paper considers voltage-dependent load models rather than simply constant power load models.

III. Load Models

This section describes the static ZIP and induction machine models considered in this paper.

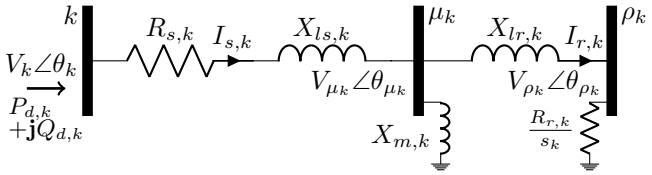

Fig. 2. Steady-state equivalent circuit of a squirrel-cage induction machine at bus k [19].

A. Controllable ZIP Model

Typical static loads are represented using a "ZIP" model which has constant impedance ("Z"), constant current ("I"), and constant power ("P") components. To incorporate demand response capabilities into the typical ZIP model, we introduce a scalar variable ε_k that represents the ratio (at a given voltage magnitude) between the controlled and nominal power demands:

$$\mathcal{F}_k^{ZP}(V_k,\varepsilon_k) = \varepsilon_k P_{d,k}^0 \left[a_{1,k}\left(\frac{V_k}{V_k^0}\right)^2 + a_{2,k}\left(\frac{V_k}{V_k^0}\right) + a_{3,k}\right], \tag{1a}$$

$$\mathcal{F}_k^{ZQ}(V_k,\varepsilon_k) = \varepsilon_k Q_{d,k}^0 \left[b_{1,k}\left(\frac{V_k}{V_k^0}\right)^2 + b_{2,k}\left(\frac{V_k}{V_k^0}\right) + b_{3,k}\right], \tag{1b}$$

where $\mathcal{F}_k^{ZP}$ and $\mathcal{F}_k^{ZQ}$ are the functions representing the real and reactive power consumption of the controllable ZIP model, $P_{d,k}^0$ and $Q_{d,k}^0$ are the nominal real and reactive demands, and V_k^0 is the nominal voltage magnitude at load bus k. The coefficients $a_{1,k}$, $a_{2,k}$, and $a_{3,k}$ represent constant impedance, constant current, and constant power fractions for real power. Corresponding reactive power coefficients are denoted $b_{1,k}$, $b_{2,k}$, and $b_{3,k}$. These coefficients sum to one, i.e., $\sum_{i=1}^3 a_{i,k} = 1$ and $\sum_{i=1}^3 b_{i,k} = 1$ for all k.

B. Induction Machine Model

Fig. 2 shows the equivalent circuit of a squirrel-cage induction machine. An induction machine at bus k is modeled using two additional internal buses denoted μ_k and ρ_k along with a "slip" variable s_k indicating the normalized difference between the electrical frequency and the induction machine's mechanical speed. A slip equal to 1 indicates zero mechanical speed, while a slip equal to 0 indicates that the machine operates at synchronous speed. For both $s_k = 0$ and $s_k = 1$, the induction machine delivers zero mechanical power but may consume electrical power due to losses. Fig. 3 shows an induction machine's power consumption as a function of s_k.

Based on the circuit in Fig. 2, the real and reactive demands at bus k become functions of the voltage phasors at buses k, μ_k and ρ_k as well as the machine's slip:

$$P_{d,k} + jQ_{d,k} = V_k e^{j\theta_k}\left(\frac{V_{\mu,k}e^{j\theta_{\mu,k}}}{jX_{m,k}} + \frac{V_{\rho,k}e^{j\theta_{\rho,k}}s_k}{R_{r,k}}\right)^*, \tag{2}$$

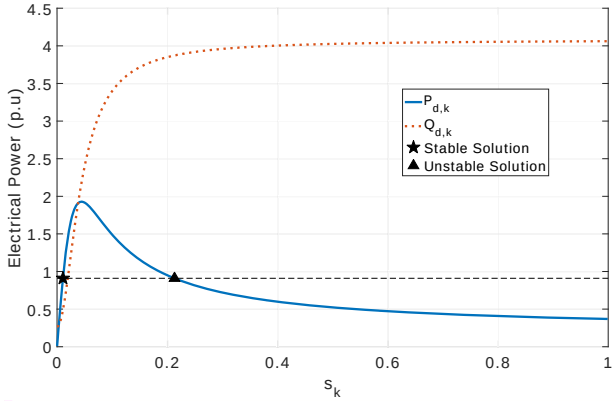

Fig. 3. The electrical power consumption of an induction machine as a function of the slip.

where $j = \sqrt{-1}$. Splitting (2) into real and imaginary components yields

$$\mathcal{F}_k^{IP}(\theta_k, V_k, \theta_{\mu,k}, V_{\mu,k}, \theta_{\rho,k}, V_{\rho,k}, s_k) = \frac{V_k V_{\mu,k}}{X_{m,k}}\sin(\theta_{\mu,k} - \theta_k) + \frac{V_k V_{\rho,k} s_k}{R_{r,k}}\cos(\theta_{\rho,k} - \theta_k), \tag{3a}$$

$$\mathcal{F}_k^{IQ}(\theta_k, V_k, \theta_{\mu,k}, V_{\mu,k}, \theta_{\rho,k}, V_{\rho,k}, s_k) = \frac{V_k V_{\mu,k}}{X_{m,k}}\cos(\theta_{\mu,k} - \theta_k) - \frac{V_k V_{\rho,k} s_k}{R_{r,k}}\sin(\theta_{\rho,k} - \theta_k). \tag{3b}$$

The voltage magnitudes are related by Ohm's law:

$$V_k e^{j\theta_k} - V_{\mu,k}e^{j\theta_{\mu,k}} = (R_{s,k} + jX_{ls,k})\left(\frac{V_{\mu,k}e^{j\theta_{\mu,k}}}{jX_{m,k}} + \frac{V_{\rho,k}e^{j\theta_{\rho,k}}s_k}{R_{r,k}}\right), \tag{4a}$$

$$V_{\mu,k}e^{j\theta_{\mu,k}} = V_{\rho,k}e^{j\theta_{\rho,k}}\left(1 + jX_{lr,k}\frac{s_k}{R_{r,k}}\right). \tag{4b}$$

As shown in Fig. 3, for a specific value of real power demand $P_{d,k}$ and terminal voltage magnitude V_k (the horizontal dashed line), there can exist multiple possible values for the slip s_k. We choose the smallest slip, which corresponds to stable operation (the star), by imposing the limits $\underline{s}_k \le s_k \le \overline{s}_k$. Since the induction machine represents a load, the slip should be greater than zero; therefore, we impose a small nonzero value as the lower limit $\underline{s}_k$. The value of the upper limit $\overline{s}_k$, which must be small enough to preclude unstable solutions, depends on the machine parameters.

We consider a composite load model, which allows for the combination of both ZIP loads and induction machine loads:

$$S_{d,k} = (1-\alpha)S_{\text{ZIP},k} + \alpha S_{\text{IM},k} \tag{5}$$

where S_{ZIP} and S_{IM} represent the complex power demands of the ZIP load and the induction machine, respectively, and α is the percentage of induction machine load ($0 \le \alpha \le 1$).

IV. Optimization Formulation

Our recent work [11] proposes a non-convex optimization formulation for determining loading patterns that improve voltage stability as measured by the SSV of the power flow

Jacobian matrix. This section introduces ZIP and induction machine models into this formulation.

A. Jacobian Matrix

The standard AC power flow equations [20] are used to compute the conventional power flow Jacobian matrix:

$$\mathcal{F}_i^P(\boldsymbol{\theta}, \boldsymbol{V}) = V_i \sum_{j \in \mathcal{N}} V_j (G_{ij} \cos\theta_{ij} + B_{ij} \sin\theta_{ij}), \quad (6a)$$

$$\mathcal{F}_i^Q(\boldsymbol{\theta}, \boldsymbol{V}) = V_i \sum_{j \in \mathcal{N}} V_j (G_{ij} \sin\theta_{ij} - B_{ij} \cos\theta_{ij}), \quad (6b)$$

where $\theta_{ij} = \theta_i - \theta_j$, $G_{ij} = \mathrm{Re}(Y_{ij})$, and $B_{ij} = \mathrm{Im}(Y_{ij})$. The conventional Jacobian matrix is an $m \times m$ matrix, where $m = n_{\mathrm{pv}} + 2n_{\mathrm{pq}}$:

$$J_{\mathrm{cnv}} = \begin{bmatrix} \frac{\partial \mathcal{F}_i^P}{\partial \theta_i} & \frac{\partial \mathcal{F}_i^P}{\partial V_j} \\ \frac{\partial \mathcal{F}_j^Q}{\partial \theta_i} & \frac{\partial \mathcal{F}_j^Q}{\partial V_j} \end{bmatrix}, \quad (7)$$

where each term represents a submatrix of partial derivatives over the indices $i \in \{\mathcal{S}_{\mathrm{PV}}, \mathcal{S}_{\mathrm{PQ}}\}$ and $j \in \mathcal{S}_{\mathrm{PQ}}$.

Models of voltage-dependent loads result in modifications to the conventional power flow Jacobian. For a system with ZIP load models, the $m \times m$ Jacobian matrix is

$$J_{\mathrm{ZIP}} = J_{\mathrm{cnv}} + \begin{bmatrix} \mathbf{0}_{n-1 \times n-1} & \frac{\partial \mathcal{F}_i^{ZP}}{\partial V_j} \\ \mathbf{0}_{n_{\mathrm{pq}} \times n-1} & \frac{\partial \mathcal{F}_j^{ZQ}}{\partial V_j} \end{bmatrix}, \quad (8)$$

where the new terms are submatrices over the indices $i \in \{\mathcal{S}_{\mathrm{PV}}, \mathcal{S}_{\mathrm{PQ}}\}$ and $j \in \mathcal{S}_{\mathrm{PQ}}$.

The real and reactive power demands of the induction machine model are functions of the variables θ_k, $V_k, \theta_{\mu,k}$, $V_{\mu,k}$, $\theta_{\rho,k}$, $V_{\rho,k}$, s_k, $\forall k \in \mathcal{S}_{\mathrm{DR}}$. The modified $m \times m + 5n_{\mathrm{dr}}$ Jacobian matrix is

$$J_{\mathrm{IM}} = \begin{bmatrix} J_{\mathrm{cnv}} & \mathbf{0}_{m \times 5n_{\mathrm{dr}}} \end{bmatrix} + \begin{bmatrix} \frac{\partial \mathcal{F}_i^{IP}}{\partial \theta_i} & \frac{\partial \mathcal{F}_i^{IP}}{\partial V_j} & \frac{\partial \mathcal{F}_i^{IP}}{\partial \theta_{\mu,k}} & \frac{\partial \mathcal{F}_i^{IP}}{\partial V_{\mu,k}} & \frac{\partial \mathcal{F}_i^{IP}}{\partial \theta_{\rho,k}} & \frac{\partial \mathcal{F}_i^{IP}}{\partial V_{\rho,k}} & \frac{\partial \mathcal{F}_i^{IP}}{\partial s_k} \\ \frac{\partial \mathcal{F}_j^{IQ}}{\partial \theta_i} & \frac{\partial \mathcal{F}_j^{IQ}}{\partial V_j} & \frac{\partial \mathcal{F}_j^{IQ}}{\partial \theta_{\mu,k}} & \frac{\partial \mathcal{F}_j^{IQ}}{\partial V_{\mu,k}} & \frac{\partial \mathcal{F}_j^{IQ}}{\partial \theta_{\rho,k}} & \frac{\partial \mathcal{F}_j^{IQ}}{\partial V_{\rho,k}} & \frac{\partial \mathcal{F}_j^{IQ}}{\partial s_k} \end{bmatrix}, \quad (9)$$

where the new terms are submatrices over the indices $i \in \{\mathcal{S}_{\mathrm{PV}}, \mathcal{S}_{\mathrm{PQ}}\}$, $j \in \mathcal{S}_{\mathrm{PQ}}$, and $k \in \mathcal{S}_{DR}$. For example, the partial derivatives $\partial \mathcal{F}_i^{IP}/\partial \theta_{\mu,k}$, $\partial \mathcal{F}_i^{IP}/\partial \theta_{\rho,k}$, $\partial \mathcal{F}_i^{IP}/\partial V_{\mu,k}$, $\partial \mathcal{F}_i^{IP}/\partial V_{\rho,k}$, $\partial \mathcal{F}_i^{IP}/\partial s_k$ are each of size $(n-1) \times n_{\mathrm{dr}}$.

The Jacobian matrix for the composite load model is formed by the weighted sum of J_{ZIP} and J_{IM}:

$$J_{\mathrm{com}} = (1-\alpha) \begin{bmatrix} J_{\mathrm{ZIP}} & \mathbf{0}_{m \times 5n_{\mathrm{dr}}} \end{bmatrix} + \alpha J_{\mathrm{IM}}. \quad (10)$$

The SSV of a matrix is closely related to the matrix's dimension. The SSV of the sum of two matrices, as in (8), obeys the following inequality [21]:

$$\sigma_{\min}(A+B) \geq \sigma_{\min}(A) - \sigma_{\max}(B) \quad (11)$$

where $\sigma_{\min}(\cdot)$ denotes the SSV and $\sigma_{\max}(\cdot)$ the largest singular value of the corresponding matrix. Therefore, we can not say much about the relative size of the SSV of J_{cnv} versus J_{ZIP}. In contrast, appending columns to a matrix, as in (9), increases its SSV.

Theorem 1: Let $A \in \mathbb{R}^{m \times n}$, $z \in \mathbb{R}^{m \times 1}$, where $m \leq n$. Then $\sigma_{\min}(\begin{bmatrix} A & z \end{bmatrix}) \geq \sigma_{\min}(A)$.

Proof: See appendix. ∎

Therefore, the SSV of J_{IM} is larger than that of J_{cnv} at the same operating point. We discuss the implication of this result in Section V-B.

B. Smallest Singular Value Maximization Problem

The optimization problems in [9] and [10] enforce voltage stability constraints based on the SSV of the power flow Jacobian. In contrast, we wish to find the loading pattern $\boldsymbol{P_d}$ that maximizes the SSV of the modified power flow Jacobian matrix J_{com} given in (10). We exploit the fact that the singular values of a matrix A are the square roots of the eigenvalues of AA^T in order to consider the eigenvalues of the matrix $J_{\mathrm{com}}J_{\mathrm{com}}^T$ rather than explicitly form the singular values of J_{com}. This facilitates the following mathematical formalization of the problem description from Section II:

$$\max_{\substack{\boldsymbol{P_g}, \boldsymbol{Q_g}, \boldsymbol{P_d}, \boldsymbol{Q_d}, \\ \boldsymbol{V}, \boldsymbol{\theta}, \boldsymbol{V_\mu}, \boldsymbol{\theta_\mu}, \\ \boldsymbol{V_\rho}, \boldsymbol{\theta_\rho}, \boldsymbol{s}, \boldsymbol{\varepsilon}, \lambda_0}} \lambda_0 \quad \text{subject to} \quad (12a)$$

$$J_{\mathrm{com}}J_{\mathrm{com}}^T - \lambda_0 I \succeq 0 \quad (12b)$$

$$\mathcal{F}_i^P(\boldsymbol{\theta}, \boldsymbol{V}) = P_{g,i} - P_{d,i} \qquad \forall i \in \mathcal{N} \quad (12c)$$

$$\mathcal{F}_i^Q(\boldsymbol{\theta}, \boldsymbol{V}) = Q_{g,i} - Q_{d,i} \qquad \forall i \in \mathcal{N} \quad (12d)$$

$$(1-\alpha)\mathcal{F}_i^{ZP}(\cdot) + \alpha \mathcal{F}_i^{IP}(\cdot) = P_{d,i} \qquad \forall i \in \mathcal{S}_{\mathrm{DR}} \quad (12e)$$

$$(1-\alpha)\mathcal{F}_i^{ZQ}(\cdot) + \alpha \mathcal{F}_i^{IQ}(\cdot) = Q_{d,i} \qquad \forall i \in \mathcal{S}_{\mathrm{DR}} \quad (12f)$$

$$V_i \angle\theta_i - V_{\mu,i}\angle\theta_{\mu,i} = (R_{s,i} + jX_{ls,i})\, I_{s,i} \qquad \forall i \in \mathcal{S}_{\mathrm{DR}} \quad (12g)$$

$$I_{s,i} = \frac{V_{\mu,i}\angle\theta_{\mu,i}}{jX_{m,i}} + \frac{V_{\rho,i}\angle\theta_{\rho,i} s_i}{R_{r,i}} \qquad \forall i \in \mathcal{S}_{\mathrm{DR}} \quad (12h)$$

$$V_{\mu,i}\angle\theta_{\mu,i} = V_{\rho,i}\angle\theta_{\rho,i} \left(1 + j\frac{X_{lr,i} s_i}{R_{r,i}}\right) \qquad \forall i \in \mathcal{S}_{\mathrm{DR}} \quad (12i)$$

$$\textstyle\sum_{i \in \mathcal{S}_{\mathrm{DR}}} P_{d,i} = \sum_{i \in \mathcal{S}_{\mathrm{DR}}} P_{d,i}^0 \quad (12j)$$

$$P_{d,i} = P_{d,i}^0 \qquad \forall i \in \mathcal{S}_{\mathrm{PQ}} \setminus \mathcal{S}_{\mathrm{DR}} \quad (12k)$$

$$P_{g,i} = P_{g,i}^0 \qquad \forall i \in \mathcal{S}_{\mathrm{PV}} \quad (12l)$$

$$V_i = V_i^0 \qquad \forall i \in \mathcal{S}_{\mathrm{PV}} \quad (12m)$$

$$V_{\mathrm{ref}} = V_{\mathrm{ref}}^0,\ \theta_{\mathrm{ref}} = 0 \quad (12n)$$

$$\mathcal{H}_{ij}(\boldsymbol{\theta}, \boldsymbol{V}) \leq \kappa_{ij} \quad (12o)$$

$$\mathcal{H}_{ji}(\boldsymbol{\theta}, \boldsymbol{V}) \leq \kappa_{ji} \quad (12p)$$

$$\underline{P}_{g,\mathrm{ref}} \leq P_{g,\mathrm{ref}} \leq \overline{P}_{g,\mathrm{ref}} \quad (12q)$$

$$\underline{Q}_{g,\mathrm{ref}} \leq Q_{g,\mathrm{ref}} \leq \overline{Q}_{g,\mathrm{ref}} \quad (12r)$$

$$\underline{Q}_{g,i} \leq Q_{g,i} \leq \overline{Q}_{g,i} \qquad \forall i \in \mathcal{S}_{\mathrm{PV}} \quad (12s)$$

$$\underline{P}_{d,i} \leq P_{d,i} \leq \overline{P}_{d,i} \qquad \forall i \in \mathcal{S}_{\mathrm{DR}} \quad (12t)$$

$$\underline{s}_i \leq s_i \leq \overline{s}_i \qquad \forall i \in \mathcal{S}_{\mathrm{DR}} \quad (12u)$$

$$\underline{V}_i \leq V_i \leq \overline{V}_i \qquad \forall i \in \mathcal{S}_{\mathrm{PQ}} \quad (12v)$$

The combination of the objective (12a) and constraint (12b) ensures that λ_0 is the smallest eigenvalue of the matrix $J_{\mathrm{com}}J_{\mathrm{com}}^T$. Constraints (12c) and (12d) are the standard nonlinear AC power flow equations. Constraints (12e) and (12f) are the real and reactive power demands of the demand-responsive loads. Constraints (12g)–(12i) are the

electrical equations for the steady-state induction machine model. While demands at the load buses without demand-responsive loads can be treated using any appropriate load model, our numerical results assume a constant power load model for simplicity. Constraint (12j) ensures that the total demand-responsive load is constant, (12k)–(12n) fix the non-responsive loads' real power demands, the generators' real power production at PV buses, voltage magnitudes at all generator buses, and the voltage angle at the reference bus. Constraints (12o)–(12v) enforce the upper limits of power flows on the branches (in terms of apparent power) as well as upper and lower limits on real power and reactive power production at the reference bus, reactive power production at PV buses, real power demands of demand-responsive loads (which is a function of demand flexibility in both the current time period and the payback period), slips of the induction machines, and voltage magnitudes at PQ buses.

C. Solution Approach

We adapt the iterative linear programming algorithm presented in [11] to solve (12). This algorithm relies on linearizations of the objective function and constraints in (12).

To address (12b), the linear sensitivity of the smallest eigenvalue is derived using eigenvalue sensitivities [22]:

$$\frac{\partial \lambda_0}{\partial \chi} = w_0^T \frac{\partial (J_{\text{com}} J_{\text{com}}^T)}{\partial \chi} u_0, \tag{13}$$

where χ represents the system states and w_0 and u_0 are the normalized left and right eigenvectors corresponding to the smallest eigenvalue λ_0 of $J_{\text{com}} J_{\text{com}}^T$. A change in the states χ yields an approximate change in λ_0 that is given by

$$\Delta\lambda_0 = \sum_i w_0^T \frac{\partial (J_{\text{com}} J_{\text{com}}^T)}{\partial \chi_i} u_0 \Delta\chi_i. \tag{14}$$

The relevant system states for the ZIP model are

$$\chi_{\text{ZIP}} = [\theta_i, V_j, \varepsilon_k\ ]^T \tag{15}$$

and for the IM model are

$$\chi_{\text{IM}} = [\theta_i, V_j, \theta_{\mu,k}, V_{\mu,k}, \theta_{\rho,k}, V_{\rho,k}, s_k]^T, \tag{16}$$

where $i \in \{\mathcal{S}_{\text{PV}}, \mathcal{S}_{\text{PQ}}\}$, $j \in \mathcal{S}_{\text{PQ}}$, and $k \in \mathcal{S}_{\text{DR}}$. In addition to (12b), the iterative linear programming algorithm requires linearization of the AC power flow and load model equations, which is accomplished via first-order Taylor expansion.

After evaluating these linearizations at the approximate solution from the previous iteration, each iteration of the algorithm solves the following linear optimization problem:

$$\max_{\substack{\Delta \boldsymbol{P}_g, \Delta \boldsymbol{Q}_g, \Delta \boldsymbol{P}_d, \\ \Delta \boldsymbol{Q}_d, \Delta \boldsymbol{V}, \Delta \boldsymbol{\theta}, \\ \Delta \boldsymbol{V_\mu}, \Delta \boldsymbol{\theta_\mu}, \boldsymbol{V_\rho}, \\ \Delta \boldsymbol{\theta_\rho}, \Delta \boldsymbol{s}, \Delta \boldsymbol{\varepsilon}, \Delta\lambda_0}} \quad \Delta\lambda_0 \quad \text{subject to} \tag{17a}$$

$$\begin{aligned}
\Delta\lambda_0 = {} & \textstyle\sum_i \left[w_0^T \frac{\partial (J_{\text{com}} J_{\text{com}}^T)}{\partial \theta_i} u_0 \right] \Delta\theta_i \\
& + \textstyle\sum_j \left[w_0^T \frac{\partial (J_{\text{com}} J_{\text{com}}^T)}{\partial V_j} u_0 \right] \Delta V_j \\
& + \textstyle\sum_k \left[w_0^T \frac{\partial (J_{\text{com}} J_{\text{com}}^T)}{\partial \theta_{\mu,k}} u_0 \right] \Delta\theta_{\mu,k} \\
& + \textstyle\sum_k \left[w_0^T \frac{\partial (J_{\text{com}} J_{\text{com}}^T)}{\partial \theta_{\rho,k}} u_0 \right] \Delta\theta_{\rho,k} \\
& + \textstyle\sum_k \left[w_0^T \frac{\partial (J_{\text{com}} J_{\text{com}}^T)}{\partial V_{\mu,k}} u_0 \right] \Delta V_{\mu,k} \\
& + \textstyle\sum_k \left[w_0^T \frac{\partial (J_{\text{com}} J_{\text{com}}^T)}{\partial V_{\rho,k}} u_0 \right] \Delta V_{\rho,k} \\
& + \textstyle\sum_k \left[w_0^T \frac{\partial (J_{\text{com}} J_{\text{com}}^T)}{\partial \varepsilon_k} u_0 \right] \Delta\varepsilon_k \\
& + \textstyle\sum_k \left[w_0^T \frac{\partial (J_{\text{com}} J_{\text{com}}^T)}{\partial s_k} u_0 \right] \Delta s_k
\end{aligned}$$

$$i \in \{\mathcal{S}_{\text{PV}}, \mathcal{S}_{\text{PQ}}\}, \forall j \in \mathcal{S}_{\text{PQ}}, \forall k \in \mathcal{S}_{\text{DR}} \tag{17b}$$

$$\text{Linearizations of (12c)–(12v)} \tag{17c}$$

$$\Delta\lambda_0 \leq \overline{\Delta\lambda}_0 \tag{17d}$$

where (17b) is the linear eigenvalue sensitivity constraint corresponding to the composite load model. Constraint (17d) limits the step size of $\Delta\lambda_0$ to ensure the accuracy of the linearization.

We extend the *iterative sensitivity SSV algorithm* presented in [11] to include J_{com}, as follows.

Algorithm 1 Extended Iterative Sensitivity SSV

Input: The nominal operating point χ^0

1: $iter \leftarrow 0$
2: $\chi^{iter} = \chi^0$
3: **repeat**
4: Compute (17b)–(17d) at χ^{iter}
5: Solve (17) at χ^{iter} to obtain $\Delta \boldsymbol{P}_d^{opt}$, $\Delta \boldsymbol{Q}_d^{opt}$, $\Delta\lambda_0$
6: $iter \leftarrow iter + 1$
7: $\boldsymbol{P}_d^{iter} = \boldsymbol{P}_d^{iter-1} + \Delta \boldsymbol{P}_d^{opt}, \boldsymbol{Q}_d^{iter} = \boldsymbol{Q}_d^{iter-1} + \Delta \boldsymbol{Q}_d^{opt}$
8: Solve (6) to obtain a new χ^{iter}
9: **until** $\Delta\lambda_0 < 10^{-5}$

Output: $\boldsymbol{P}_d^{iter}$, λ_0^{iter}

The solution to (17) provides an approximation of the change in decision variables that leads to the maximum increase in λ_0, within the region near the linearization point. Each iteration of the extended algorithm refines an approximate solution to (12) by linearizing around the previous operating point, solving (17), adding the changes provided by that solution of (17) to the previous operating point, and solving the AC power flow equations (6) to obtain a new operating point. The algorithm terminates when $\Delta\lambda_0$ is less than a specified threshold (here, 10^{-5}).

V. Results and Discussion

This section describes the results of case studies conducted on the IEEE 14-bus system available in MATPOWER [23]. We assume the loads at buses 4, 9, and 14 are demand-responsive resulting in 92.2 MW of responsive demand out of 259 MW of total demand.

We set $\overline{\Delta\lambda}_0 = 0.01$ and list the parameters of the induction machine models in Table I. The upper bounds of the slips are determined based on the induction machine parameters. For example, the relationship between the power

TABLE I

INDUCTION MACHINE PARAMETERS (P.U.) [19]

Bus #	R_s	X_{ls}	R_r	X_{lr}	X_m	$\overline{s}$
4	0.012	0.07	0.01	0.17	3.5	0.04
9	0.001	0.23	0.015	0.23	5.8	0.03
14	0.001	0.23	0.015	0.23	5.8	0.03

TABLE II

ZIP LOAD MODELS COEFFICIENTS [16], [17]

Types	a_1	a_2	a_3	b_1	b_2	b_3
Air conditioner	1.17	-1.83	1.66	15.68	-27.15	12.47
Battery charger	3.51	-3.94	1.43	5.80	-7.26	2.46
Baseboard heater	1.00	0.00	0.00	0.00	0.00	0.00
Dryer	1.91	-2.24	1.33	2.51	-2.34	0.83
Refrigerator/freezer	1.19	-0.26	0.07	0.59	0.65	-0.24
Heat pump	0.84	-1.40	1.56	22.92	-40.39	18.47
Washing machine	0.05	0.32	0.63	-0.56	2.20	-0.64

consumption and slip of the machine at bus 4 is shown in Fig. 3. Since the peak real power consumption occurs when the slip equals 0.04 we set $\overline{s}_4 = 0.04$ to ensure the algorithm finds the stable operating point. We set $\underline{s}_k = 0.0001$, $\forall k \in \mathcal{S}_{\text{DR}}$. The ZIP coefficients for a variety of loads typically used for demand response are given in Table II.

The nominal consumption of the loads at buses 4, 9, and 14 along with the SSV of J_{cnv} is given in Table III (see Nominal, Constant Power, J_{cnv}). Modeling the loads as constant power loads with fixed power factors (as in [11]) and applying the iterative sensitivity SSV algorithm, we obtain the optimal loading pattern shown in Table III (see Optimal for 3 DR buses, Constant Power, J_{cnv}). All of demand-responsive load is shifted to bus 4, improving the SSV by 0.97%. The remaining values in Table III will be discussed later.

A. Controllable ZIP Model

We first consider cases where all demand-responsive loads are modeled as having only one ZIP component. Fig. 4 illustrates the results obtained by applying the iterative sensitivity SSV algorithm to each case, where the matrix in the figure defines the cases (e.g., ZIP case #9 corresponds to a constant real/reactive power load model). The nominal SSVs are different since J_{ZIP} is different in each case. The optimal real power loading pattern is the same in all cases: $[P_{d,4}\ P_{d,9}\ P_{d,14}] = [92.2\ 0\ 0]$ MW. However, the reactive power demand at bus 4 is different in each case since the load's power factor is a function of the voltage magnitude in ZIP cases #1-8. Table III shows the results for case #3 (see Optimal for 3 DR buses, ZIP, J_{ZIP}), which produces the largest SSV. However, ZIP case #9 produces the largest percent improvement: 0.974%.

We next model the demand-responsive loads using the ZIP coefficients in Table II. In each case, we model all demand-responsive load as a single type of load (i.e., using one set of ZIP coefficients). Results are shown in Fig. 5. The baseboard heater model produces the largest SSV but the smallest percentage improvement. Again, the constant

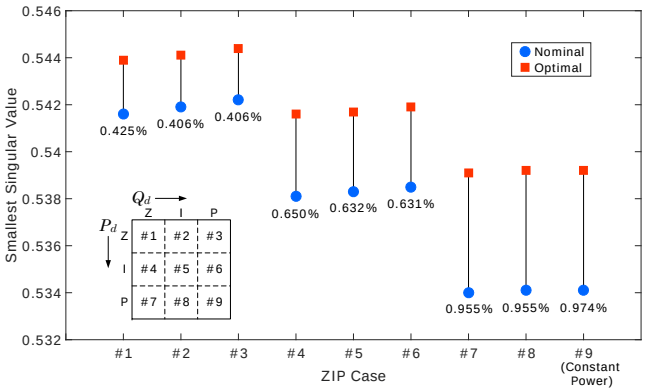

Fig. 4. The nominal and optimal SSV for different ZIP cases, as shown in the matrix. The values below the blue circles are the percent improvements.

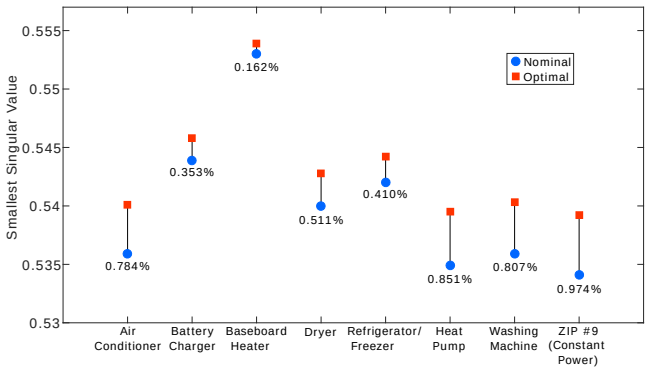

Fig. 5. The nominal and optimal SSV for common demand-responsive loads. The values below the blue circles are the percent improvements.

power load model (corresponding to ZIP case #9) produces the largest percent improvement.

B. Induction Machine Model

We now model each load as an induction machine (representing the aggregation of a large number of smaller machines) using the parameters given in Table I. The SSV increases from 2.3360 to 2.4533 (5% improvement). The nominal SSV is larger than the nominal SSVs associated with the ZIP loads as expected from Theorem 1.

The optimal loading pattern is shown in Table III (see Optimal for 3 DR buses, IM, J_{IM}). The limits on the induction machines' slips prevent the real power demand at buses 9 and 14 from going to zero, but the optimal loading pattern is similar to the cases with ZIP loads: almost all of the demand-responsive load is shifted to bus 4. However, unlike in the ZIP model cases, the reactive demands at buses 9 and 14 are much greater than zero when the real power demand is close to zero, which is an inherent characteristic of typical induction machines, as shown in Fig. 3.

To consider the possibility of disconnecting the induction machines at low consumption levels, we modify the algorithm with the following logical condition: if an induction machine's real power demand at any iteration is less than 0.01 p.u., we disconnect the induction machine by setting its real and reactive power demand to zero prior to continuing the algorithm. Fig. 6 illustrates the impacts of this modification. At approximately 50 iterations, P_d at bus 14 is less

TABLE III

LOADING PATTERN COMPARISON, P_d IN MW AND Q_d IN MVAR

Load Model Jacobian	Nominal Constant Power J_{cnv}		Optimal for 3 DR buses Constant Power J_{cnv}		ZIP #3 J_{ZIP}		ZIP #3 J_{cnv}		IM J_{IM}		IM J_{cnv}		Optimal for 2 DR buses ZIP #3 J_{ZIP}		IM J_{IM}	
	P_d	Q_d	P_d	Q_d	P_d	Q_d	P_d	Q_d	P_d	Q_d	P_d	Q_d	P_d	Q_d	P_d	Q_d
Bus 4	47.80	32.62	92.20	62.90	92.20	63.99	92.20	63.99	90.99	48.90	71.28	39.94	92.20	63.99	80.81	43.94
Bus 9	29.50	20.73	0.00	0.00	0.00	0.00	0.00	0.00	0.62	15.55	20.34	18.50	0.00	0.00	11.39	17.51
Bus 14	14.90	16.39	0.00	0.00	0.00	0.00	0.00	0.00	0.59	15.79	0.59	15.73	-	-	-	-
SSV	0.5341		0.5393		0.5444		0.5391		2.4533		0.5369		0.5444		2.184	

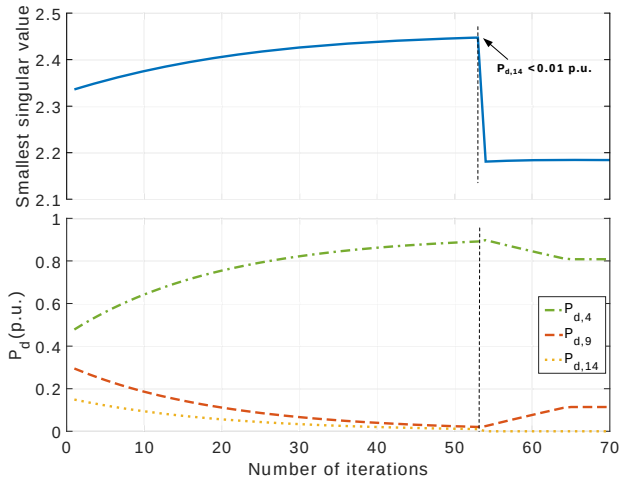

Fig. 6. Convergence of the SSV and real power demand of the demand-responsive loads if the induction machine at bus 14 is disconnected at low loading.

than 0.01 p.u. (as shown by the vertical dashed lines), so the algorithm disconnects the induction machine at bus 14. After another 15 iterations, the algorithm reaches the optimum; however, the optimum is not what we would expect given the convergence trajectory before the machine was disconnected. Instead of shifting all load to bus 4, the optimal loading pattern keeps some load at bus 9, as shown in Fig. 6 and Table III (see Optimal for 2 DR buses, IM, J_{IM}), which is different than results obtained using ZIP models within a system with no load at bus 14 and demand-responsive loads at buses 4 and 9 (see Optimal for 2 DR buses, ZIP, J_{ZIP}). Disconnecting the induction machine at bus 14 reduces the number of columns of J_{IM}. According to Theorem 1, this leads to a decrease in the the SSV, in this case, from 2.447 to 2.181 prior to converging to a new optimum 2.184, as shown in Fig. 6.

C. Composite Load Model

Table IV summarizes the nominal and optimal SSV results for several ZIP models (including ZIP case #3, which has the largest optimal SSV), the induction machine model, and two composite load models. In addition to the SSVs, we report the absolute improvement (Δ) and percent improvement (%). The case using induction machine models alone has the largest absolute and percent improvement.

TABLE IV

SSV COMPARISON

Load Model	Nominal	Optimal	Δ	%
Constant Power (ZIP #9)	0.5341	0.5393	0.0052	0.98
ZIP #3	0.5442	0.5444	0.0002	0.04
Induction Machine	2.3360	2.4533	0.1173	5.02
70% IM + 30% ZIP #3	2.2994	2.4078	0.1084	4.71
30% IM + 70% ZIP #3	2.2402	2.3383	0.0981	4.37

D. Difficulties in Interpreting the SSV

It is difficult, if not impossible, to compare the SSVs associated with systems that use different load models. For example, when the SSV drops in Fig. 6, it does not necessarily mean that the system is operating closer to instability. The drop is due to structural changes in the Jacobian matrix.

Instead of maximizing the SSV of J_{com}, which is structurally different for each load model, we explore the idea of maximizing the SSV of J_{cnv}, while still using J_{com} to compute the power flow. The benefit of this approach is that the nominal SSVs are identical and the optimal SSVs are comparable. The drawback is that the SSV of J_{cnv} does not reflect the physical system (unless all loads are constant power loads, in which case $J_{\text{com}} = J_{\text{cnv}}$).

Fig. 7 shows the results of maximizing J_{cnv} for ZIP cases #1-9, the induction machine model, and a composite load model. The optimal loading patterns corresponding to ZIP case #3 and the induction machine model are shown in Table III (see Optimal for 3 DR buses, ZIP #3, J_{cnv} and Optimal for 3 DR buses, IM, J_{cnv}). ZIP case #3 yields the same optimal loading patterns regardless of the choice of Jacobian matrix (J_{cnv} or J_{ZIP}) used for the SSV calculation; however, the choice of Jacobian matrix (J_{cnv} or J_{IM}) does affect the optimal loading pattern obtained when using the induction machine model. Interestingly, the SSV percent improvement when maximizing the SSV of J_{cnv} is worst with the induction machine model whereas it was the best when maximizing the SSV of J_{com} (which equals J_{IM} for the induction machine model).

E. Computation Time

All computations were implemented in MATLAB on a computer with an Intel(R) i5-6600K CPU and 8 GB of RAM. Using the ZIP model, the total time required by the iterative algorithm is less than two seconds for each test case. Using the induction machine model, the algorithm requires more time (approximately 20 seconds) because 1) the Jacobian

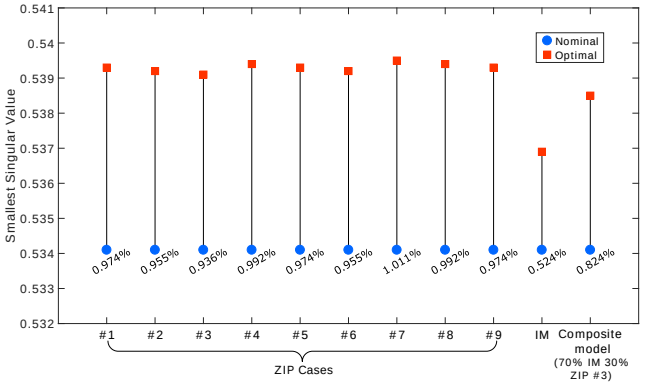

Fig. 7. The nominal and optimal SSV of the conventional Jacobian matrix. The values below the blue circles are the percent improvement.

matrix is larger requiring more time to compute the eigenvalue sensitivities, and 2) the AC power flow equations are more complex. See [11] for further discussion on how the computation time scales with system size.

VI. Conclusion

This paper incorporated two voltage-dependent load models into an algorithm for improving a static voltage stability margin based on the SSV of the power flow Jacobian matrix. An iterative linear programming technique was used to determine the optimal loading pattern that maximizes the SSV. Using the IEEE 14-bus system, we studied the impact of the load models on the optimal SSV of the full power flow Jacobian matrix (including terms corresponding to the voltage-dependent load models) and the corresponding optimal loading patterns. We found that use of different ZIP models resulted in the same optimal loading patterns, but use of induction machine models changed the optimal loading pattern, pointing to the importance of properly modeling loads when implementing such an algorithm. Comparing SSVs across systems with different load models proved difficult since structural changes in the power flow Jacobian matrix affect the magnitude of the SSV. Therefore, we also explored the impact of maximizing the SSV of the conventional Jacobian matrix, which is the same for each load model but does not reflect the physical system. This work raises the question of how to compare static voltage stability margins across systems with structural differences.

Appendix I
Proof of the Theorem 1

Proof: Let $B = \begin{bmatrix} A & z \end{bmatrix}$. Then, $BB^T = \begin{bmatrix} A & z \end{bmatrix}\begin{bmatrix} A & z \end{bmatrix}^T = AA^T + zz^T$. Let v_n be the normalized right eigenvector ($\|v_n\|_2 = 1$) corresponding to the smallest eigenvalue $\lambda_{\min}$ of BB^T, which is equal to the square of the SSV of the matrix B, i.e., $(\sigma_{\min}(B))^2$. Then,

$$\begin{aligned}(AA^T + zz^T)v_n &= (\sigma_{\min}(B))^2 v_n,\\ v_n^T(AA^T + zz^T)v_n &= (\sigma_{\min}(B))^2.\end{aligned}$$

Since zz^T is a positive semidefinite matrix, i.e., $v_n^T zz^T v_n \geq 0$, then

$$(\sigma_{\min}(B))^2 \geq v_n^T AA^T v_n \geq \|v_n^T AA^T v_n\|_2 = \|A^T v_n\|_2^2$$
$$\geq (\sigma_{\min}(A^T))^2\|v_n\|_2^2 = (\sigma_{\min}(A))^2,$$

and therefore $\sigma_{\min}\left(\begin{bmatrix} A & z \end{bmatrix}\right) \geq \sigma_{\min}(A)$. ■

References

[1] D. S. Callaway and I. A. Hiskens, "Achieving controllability of electric loads," *Proc. IEEE*, vol. 99, no. 1, pp. 184–199, 2011.

[2] J. Short, D. Infield, and L. Freris, "Stabilization of grid frequency through dynamic demand control," *IEEE Trans. Power Syst.*, vol. 22, no. 3, pp. 1284–1293, 2007.

[3] D. Callaway, "Tapping the energy storage potential in electric loads to deliver load following and regulation, with application to wind energy," *Energy Conver. Management*, vol. 50, pp. 1389–1400, 2009.

[4] C. W. Taylor, "Concepts of undervoltage load shedding for voltage stability," *IEEE Trans. Power Del.*, vol. 7, no. 2, pp. 480–488, 1992.

[5] F. Echavarren, E. Lobato, L. Rouco, M. Navarrete, R. Casanova, and G. López, "A load shedding algorithm for improvement of load margin to voltage collapse," in *IEEE PowerTech, Bologna*, June 2003.

[6] R. J. Thomas and A. Tiranuchit, "Voltage instabilities in electric power networks," in *18^{th} Southeast Symp. Syst. Theory*, 1986, pp. 359–363.

[7] A. Tiranuchit and R. Thomas, "A posturing strategy against voltage instabilities in electric power systems," *IEEE Trans. Power Syst.*, vol. 3, no. 1, pp. 87–93, 1988.

[8] P.-A. Lof, T. Smed, G. Andersson, and D. Hill, "Fast calculation of a voltage stability index," *IEEE Trans. Power Syst.*, vol. 7, no. 1, pp. 54–64, 1992.

[9] C. Cañizares, W. Rosehart, A. Berizzi, and C. Bovo, "Comparison of voltage security constrained optimal power flow techniques," in *IEEE PES Summer Meeting*, vol. 3, 2001, pp. 1680–1685.

[10] R. J. Avalos, C. A. Cañizares, and M. F. Anjos, "A practical voltage-stability-constrained optimal power flow," in *IEEE PES General Meeting*, 2008.

[11] M. Yao, J. L. Mathieu, and D. K. Molzahn, "Using demand response to improve power system voltage stability margins," in *IEEE PowerTech, Manchester*, 2017.

[12] D. Karlsson and D. J. Hill, "Modelling and identification of nonlinear dynamic loads in power systems," *IEEE Trans. Power Syst.*, vol. 9, no. 1, pp. 157–166, 1994.

[13] T. Overbye, "Effects of load modelling on analysis of power system voltage stability," *Int. J. Electrical Power & Energy Syst.*, vol. 16, no. 5, pp. 329–338, 1994.

[14] I. Hiskens and J. Milanovic, "Load modelling in studies of power system damping," *IEEE Trans. Power Syst.*, vol. 10, no. 4, pp. 1781–1788, 1995.

[15] W. D. Rosehart, C. A. Cañizares, and V. H. Quintana, "Effect of detailed power system models in traditional and voltage-stability-constrained optimal power-flow problems," *IEEE Trans. Power Syst.*, vol. 18, no. 1, pp. 27–35, 2003.

[16] L. M. Hajagos and B. Danai, "Laboratory measurements and models of modern loads and their effect on voltage stability studies," *IEEE Trans. Power Syst.*, vol. 13, no. 2, pp. 584–592, 1998.

[17] A. Bokhari, A. Alkan, R. Dogan, M. Diaz-Aguiló, F. De Leon, D. Czarkowski, Z. Zabar, L. Birenbaum, A. Noel, and R. E. Uosef, "Experimental determination of the ZIP coefficients for modern residential, commercial, and industrial loads," *IEEE Trans. Power Del.*, vol. 29, no. 3, pp. 1372–1381, 2014.

[18] V. Vignesh, S. Chakrabarti, and S. Srivastava, "An experimental study on the load modelling using PMU measurements," in *IEEE PES T&D Conf. Expos.*, 2014.

[19] D. K. Molzahn, "Incorporating squirrel-cage induction machine models in convex relaxations of OPF problems," to appear in *IEEE Trans. Power Syst.*, 2017.

[20] A. J. Wood and B. F. Wollenberg, *Power Generation, Operation, and Control*. John Wiley & Sons, 2012.

[21] R. A. Horn and C. R. Johnson, "Topics in Matrix Analysis," *Cambridge University Press, New York*, 1991.

[22] T. Smed, "Feasible eigenvalue sensitivity for large power systems," *IEEE Trans. Power Syst.*, vol. 8, no. 2, pp. 555–563, 1993.

[23] R. Zimmerman, C. Murillo-Sanchez, and R. Thomas, "MATPOWER: Steady-state operations, planning, and analysis tools for power systems research and education," *IEEE Trans. Power Syst.*, vol. 26, no. 1, pp. 12–19, Feb 2011.